

# TOKEN EMBEDDINGS VIOLATE THE MANIFOLD HYPOTHESIS

MICHAEL ROBINSON<sup>1</sup>, SOURYA DEY<sup>2</sup>, TONY CHIANG<sup>3</sup>

**ABSTRACT.** A full understanding of the behavior of a large language model (LLM) requires our understanding of its input token space. If this space differs from our assumptions, our understanding of and conclusions about the LLM will likely be flawed. We elucidate the structure of the token embeddings both empirically and theoretically. We present a novel statistical test assuming that the neighborhood around each token has a relatively flat and smooth structure as the null hypothesis. Failing to reject the null is uninformative, but rejecting it at a specific token  $\psi$  implies an irregularity in the token subspace in a  $\psi$ -neighborhood,  $B(\psi)$ . The structure assumed in the null is a generalization of a manifold with boundary called a *smooth fiber bundle* (which can be split into two spatial regimes – small and large radius), so we denote our new hypothesis test as the “fiber bundle hypothesis.” Failure to reject the null hypothesis is uninformative, but rejecting it at  $\psi$  indicates a statistically significant irregularity at  $B(\psi)$ . By running our test over several open-source LLMs, each with unique token embeddings, we find that the null is frequently rejected, and so the evidence suggests that the token subspace is not a fiber bundle and hence also not a manifold. As a consequence of our findings, when an LLM is presented with two semantically equivalent prompts, if one prompt contains a token implicated by our test, the response to that prompt will likely exhibit less stability than the other.

## 1. INTRODUCTION

A core area for Artificial Intelligence (AI) research is to understand the central components of modern learning systems, e.g. large language models (LLMs), *assuming certain regularity conditions*. Extensive research efforts have been mobilized to tackle the explainability of AI question ([1]), leveraging ideas from computer science ([2, 3, 4]), information theory ([5, 6]), and theoretical physics ([7, 8, 9]), to mathematical insights from high-dimensional probability theory ([10, 11]), and algebraic and differential topology ([12, 13, 14]) either to prove mathematical guarantees or to elucidate model behavior.

In many—if not most—AI research papers, a *manifold hypothesis* is tacitly assumed, that the data are concentrated near a low curvature manifold without boundary. This assumption drives the research just as an assumption of Gaussianity would drive data modeling. It is important to test this kind of assumption before data modeling. One common strategy to perform such a test is simply “plotting the data” to ascertain the empirical distribution. Plotting high-dimensional data,

---

*Date:* <sup>1</sup>Mathematics and Statistics, American University, Washington, DC, USA,  
michaelr@american.edu

<sup>2</sup>Galois, Inc., Arlington, VA, USA, sourya@galois.com

<sup>3</sup>Department of Mathematics, University of Washington, Seattle, WA, chiang@math.washington.edu

---

however, is non-trivial, but there are statistical tests to help us understand the underlying distribution (Mann-Whitney, Kolmogorov-Smirnoff, etc.). In this paper, we provide an analogous test for the *regularity* of token embeddings.

The first layer of most LLMs is usually comprised of the token embeddings, which are vector representations of *tokens* (fragments of human language, e.g. parts of words, or numbers). Thus, a good first step to explain the behavior of an LLM is to understand its *token subspace* where these embedding vectors live. For the remainder of this paper, the term “token” used in the context of the token subspace will refer to this embedding. Numerous papers (for instance, see [15, 16, 17, 18, 19, 20, 21]) have pointed to unexpected behaviors exhibited by LLMs that hinge on subtle changes in wording and text layout between apparently similar prompts, suggesting that certain semantically similar tokens may have dramatically different neighborhoods in the token subspace. These differences in neighborhoods correspond to places where the token subspace does not behave stably as it is *irregular* at such a token. Linguistically, these irregularities may correspond to *polysemy* or *homonyms*—tokens with multiple distinct meanings ([22]).

The presence of irregularities imply small changes in language can drive large variation in the token subspace. Moreover, if the token subspace of an LLM is, in fact, *singular* (not a manifold), irregularities can persist into the output of the LLM, perhaps unavoidably and potentially even because of its architecture. This is because the input and output of LLMs are a fixed finite set of tokens yet the internal architectures of the model assume a structure resembling a Riemannian manifold: a metrizable space that locally preserves inner products. Not accounting for singularities in the token subspace may confound our understanding of the LLM’s behavior.

**1.1. Contributions.** We present three hypothesis tests that determine for a given token  $\psi$ , whether its token subspace neighborhood  $B(\psi)$  contains an irregularity, i.e. either has significantly high curvature or is singular. The tests are based on Theorem 1 that allows us to identify changes in subspace dimension that are inconsistent with the token subspace being:

1. A manifold (without boundary) with a given *embedded reach* (low reach corresponds to high curvature and *vice versa* ([23])),
2. A fibered manifold with boundary (which we call a *fiber bundle* for brevity) with the same embedded reach, estimated using small radii, and
3. A fiber bundle with the same embedded reach, estimated using large radii.

When these tests are rejected, this implies that  $\psi$  is less stable under mathematical transformations than other tokens. In Section 3.2, we show the endemic nature of these instabilities by proving that *context cannot resolve singularities persistently*. And finally, we provide conditions (Theorem 2) for when singularities can propagate into the output of an LLM for *generic* transformers.

In our work, we provide empirical evidence that the global token embedding obtained from four different LLMs cannot be a manifold due to non-constant local dimension. Because our hypothesis tests require the distances between all pairs of tokens, we need the token embedding vectors. For this reason, we conduct our analysis to four open source models of moderate size – GPT2 ([24]), Llemma7B ([25]), Mistral7B ([26]), and Pythia6.9B ([27]). We emphasize that while this paper demonstrates the manifold and fiber bundle tests on four open source LLMs, our

This material is based upon work supported by the Defense Advanced Research Projects Agency (DARPA) under Contract No. HR001124C0319. Any opinions, findings and conclusions or recommendations expressed in this material are those of the author(s) and do not necessarily reflect the views of the Defense Advanced Research Projects Agency (DARPA). Distribution Statement “A” (Approved for Public Release, Distribution Unlimited).

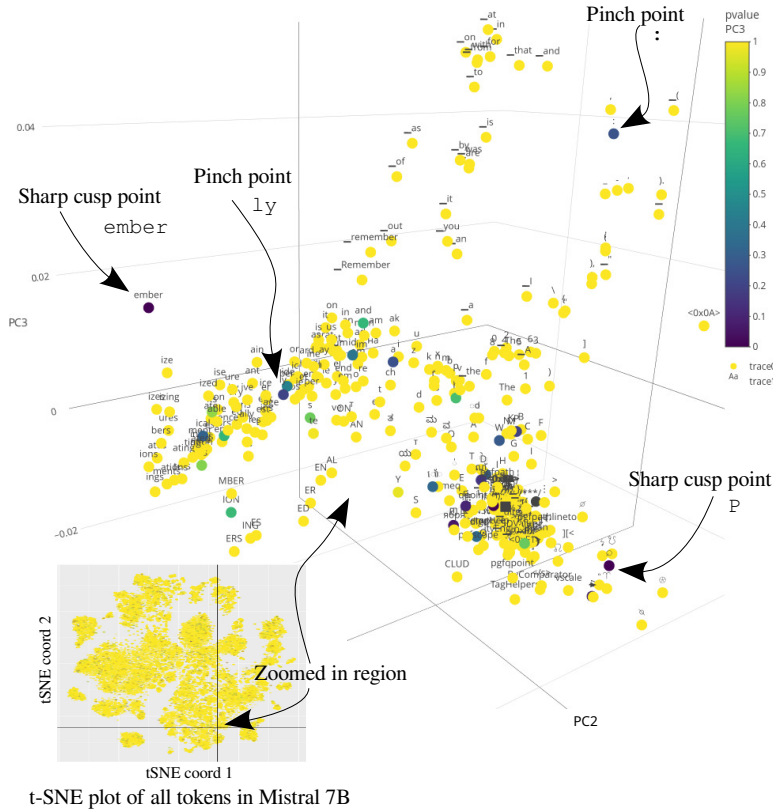


FIGURE 1. This figure shows the application of this paper’s manifold hypothesis test to a neighborhood of the token `ember` in Mistral7B. (The fiber bundle tests are not shown due to space considerations.) Since the latent space of Mistral7B has dimension  $\ell = 4096$ , we have projected the coordinates of each token shown to 3 using principal components analysis (PCA). The inset shows all of the tokens in Mistral7B (rendered with t-SNE), with a crosshairs showing the location of the zoomed-in region. Each point shown in this figure is a token used by Mistral7B, colored based upon the  $p$ -value for the manifold hypothesis test. Darker colors correspond to lower  $p$ -values, which are less consistent with the hypothesis that the token’s neighborhood is a manifold with low curvature. Putative geometric structures are labeled for certain tokens.

*main* contribution is primarily a methodology for hypothesis testing on embedded points. In particular, our method can be applied to any point cloud data set; the token embeddings we study here are merely one example.

**1.2. Background and related work.** Manifold learning takes its roots in nonlinear dimensionality reduction of high dimensional data into low dimensional representations of smooth manifolds. While these algorithms have played an important role in modern data science especially in domains such as cosmology ([28]), astrophysics

This material is based upon work supported by the Defense Advanced Research Projects Agency (DARPA) under Contract No. HR001124C0319. Any opinions, findings and conclusions or recommendations expressed in this material are those of the author(s) and do not necessarily reflect the views of the Defense Advanced Research Projects Agency (DARPA). Distribution Statement “A” (Approved for Public Release, Distribution Unlimited).

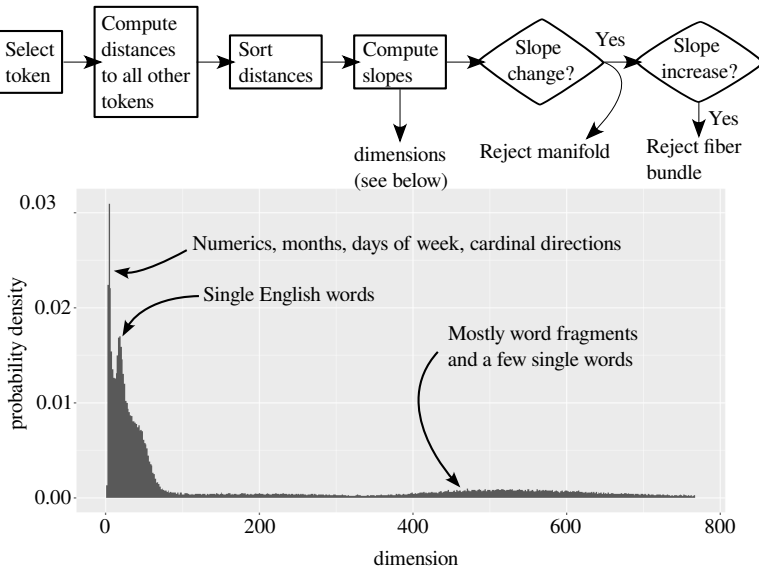


FIGURE 2. (Top) Flowchart of our statistical methodology. (Bottom) The distribution of local dimensions estimated near tokens in GPT2, produced by our method as an intermediate step. This histogram shows a mixture with at least three distinct peaks.

([29, 30]), dynamical systems ([31, 32]), and quantum chemistry ([33]), the main utility of these methods have been for data visualization. For instance, even though the Uniform Manifold Approximation and Projection (UMAP) provided an optimal algorithm for fitting sampled data to a manifold, the authors themselves concede that “if the global structure is of primary interest then UMAP may not be the best choice for dimensionality reduction” ([34]). These manifold learning algorithms will find some smooth structure to fit the data rather than “error out” when the data is not sampled from a manifold as it is not a hypothesis test. While UMAP will fit a manifold to data optimally, for instance, the manifold it finds may have extremely high curvature or dimension. Both of these are undesirable properties in a model, and both implicitly suggest that a manifold may be a poor choice for a representation. To address this concern, [35] presented a test for whether data lie on a manifold with a specified embedded reach. Unfortunately, [35] does not include the values of key constants, which makes the practical usage of this test impossible. Our paper remedies both issues: we construct a practical hypothesis test for manifolds and fiber bundles with a specified embedded reach and implement it as software.

In our test case, the basic assumption is that transformers act on the entire extrinsic latent space containing the token embedding. This is clearly a manifold as it is Euclidean. But the truth is that a transformer *in the context of an LLM* really only acts on the *embedded token subspace*. The token input embedding matrix defines this subspace, by specifying where the tokens are located. Such a space is quite unconstrained. There is no *a priori* reason to suspect it is a manifold. It has already been shown that local neighborhoods of each token have salient topological

structure ([13]), and one of the most basic parameters is the *dimension* near any given token in this space. Higher dimension at a token  $\psi$  means that  $\psi$  has greater density while lower dimensional tokens have less density ([22]). Intuitively, a densely populated  $B(\psi)$  will generically occupy a higher dimension than otherwise.

Assuming that word embeddings yield manifolds, some researchers have used global dimension estimators on token input embeddings and word embeddings ([36, 37]). By using a local (not global) dimension estimator, [38] presented the first (to our knowledge) direct test of whether the token subspace is a manifold for the token input embeddings for several LLMs, though no rigorous hypothesis test was presented. Nevertheless, a strongly negative result was obtained: the subspace of tokens is apparently never a manifold, so global dimension estimators are not reliable.

## 2. METHODS

Our method, summarized in Figures 2 and 3, proposes three related hypotheses: (1) the manifold hypothesis, (2) the fiber bundle hypothesis for small radius, and (3) the fiber bundle hypothesis for larger radius.

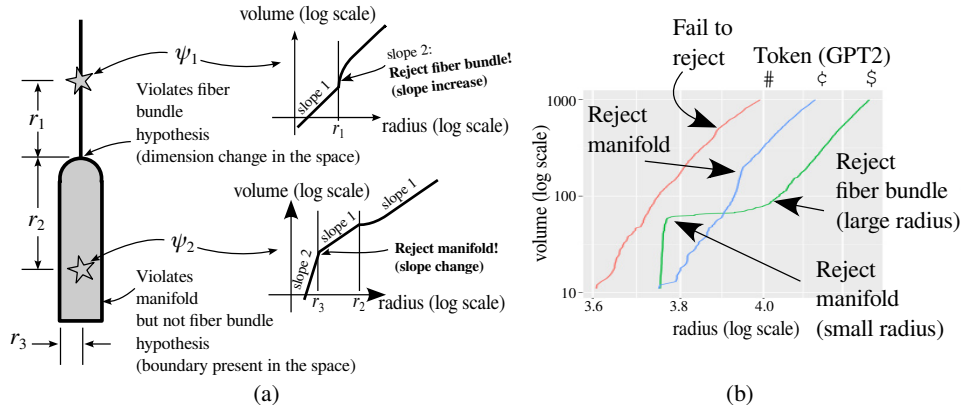


FIGURE 3. (a) Schematic of our three hypothesis tests (b) Application of the tests to the tokens #, ¢, and \$ with GPT2’s token input embedding.

The key insight is that Theorem 1 asserts that for a fiber bundle, the number of tokens within a ball of a given radius  $r$  of a fixed token is a piecewise log-log-linear function of radius, in which the slopes correspond to dimension and decrease as  $r$  increases. If there is a statistically significant change in the slope estimates (here, the significance level  $\alpha = 10^{-3}$ ), then we reject the manifold hypothesis. If there is a statistically significant *increase* in slope, then we additionally reject the fiber bundle hypothesis in the corresponding region (small or large radius).

Figure 3(b) demonstrates our method on three tokens used by GPT2. The tokens \$ and # play an important role in many programming languages, whereas ¢ does not. (Note that these tokens were chosen for illustrative purposes. The  $p$ -value for rejecting the hypotheses is larger than  $\alpha = 10^{-3}$  used in Section 3.3, so these particular tokens do not appear in any of the tables in the following sections.) The

This material is based upon work supported by the Defense Advanced Research Projects Agency (DARPA) under Contract No. HR001124C0319. Any opinions, findings and conclusions or recommendations expressed in this material are those of the author(s) and do not necessarily reflect the views of the Defense Advanced Research Projects Agency (DARPA). Distribution Statement “A” (Approved for Public Release, Distribution Unlimited).

---

token  $\#$  does not show any rejections of our hypotheses. While this does not allow one to conclude that the vicinity of  $\#$  is a manifold or fiber bundle, we can use Theorem 1 to estimate the dimension from the slope of the curve (approximately 53, once logarithms of the values on both axes are taken). The token  $\$$  exhibits a rejection of the manifold hypothesis, but not the fiber bundle hypothesis. We can conclude that there is a irregularity at a distance of roughly 3.9 units of  $\$$ . The curve for  $\$$  exhibits two slope changes at radii 3.8 and 4.0. The smaller radius slope change represents a violation of the manifold hypothesis, while the large radius slope change represents a violation of the fiber bundle hypothesis.

### 3. RESULTS

**3.1. Volume versus radius for fiber bundles.** The learned token embedding vectors in an LLM each have the same number of elements, which we refer to as  $\ell$ . Thus, the explicit representation of the token subspace  $T$  used by an LLM arises by embedding  $T$  within the *latent space*  $\mathbb{R}^\ell$  by way of a smooth function  $e : T \rightarrow \mathbb{R}^\ell$ . Since embeddings are bijective, each  $\psi \in T$  corresponds to a unique element  $e(\psi) \in \mathbb{R}^\ell$ . With a slight abuse of notation, we can write  $\psi \in e(T)$ .

The fiber bundle model imposes a specific assumption about the structure on  $T$ , by relating it to another, lower dimensional, manifold  $S$ , called the *base space*, via a smooth map  $p : T \rightarrow S$ .

**Definition 1.** A *fibered manifold* is a surjective function  $p : T \rightarrow S$  such that the Jacobian matrix  $J_{\psi}p$  at every point  $\psi \in T$  has rank equal to the dimension of  $S$ . For brevity, we refer to this kind of space simply as a *fiber bundle*.

If a fiber bundle is the correct representation of the space of tokens  $T$ , then the probability distribution of tokens given by the volume form  $v$  on  $T$  will impact the distribution of tokens within  $\mathbb{R}^\ell$ .

**Theorem 1.** Suppose that  $T$  is a compact, finite-dimensional Riemannian manifold with boundary<sup>1</sup>, with a volume form  $v$  satisfying  $v(T) < \infty$ , and let  $p : T \rightarrow S$  be a fibered manifold. If  $e : T \rightarrow \mathbb{R}^\ell$  is a smooth embedding with reach  $\tau$ , then there is a function  $\rho : e(T) \rightarrow [0, \tau]$  such that if  $\psi \in e(T)$ , the induced volume  $(e_*v)$  in  $\mathbb{R}^\ell$  satisfies

$$(1) \quad (e_*v)(B_r(\psi)) = \begin{cases} O(r^{\dim T}) & \text{if } 0 \leq r \leq \rho(\psi), \\ (e_*v)(B_{\rho(\psi)}(\psi)) + O((r - \rho(\psi))^{\dim S}) & \text{if } \rho(\psi) \leq r, \end{cases}$$

where  $B_r(\psi)$  is the ball of radius  $r$  centered at  $\psi$ , and the asymptotic limits are valid for small  $r$ .

*Proof.* See Section A.4 □

Theorem 1 characterizes the resulting probability distribution using parameters (the exponents in Equation (1)) that can be estimated from the token input embedding. These parameters are bounded by the dimensions of  $S$  and  $T$ .

In short, if we take the logarithm of both the volume and radius in Equation (1), we obtain a piecewise linear curve, in which the slopes are given by  $\dim S < \dim T$ , and the slopes must decrease through a discontinuity as the radius increases, as shown in Figure 3(a).

---

<sup>1</sup>Every point in a *manifold with boundary* has a neighborhood that is locally homeomorphic to a half-space. As a consequence, manifolds are a special case of manifolds with boundary.

---

**3.2. Context does not persistently resolve singularities.** Given a context window of  $w - 1$  tokens, an LLM uses its learned parameters to predict the next ( $w$ -th) token. This gets added to the context window and the process continues. (See Section A.1 for details.) In this section, we provide a mathematical argument showing that the use of context is insufficient to resolve singularities present in the token subspace for a generic transformer in a persistent manner. Again, denote the token subspace by  $T$ , noting that Section 3.3 shows that  $T$  is unlikely to be a manifold for typical LLMs. Let us begin with a lemma:

**Lemma 1.** *If  $X$  is a manifold,  $Y$  is an arbitrary topological space, and  $X \times Y$  is a manifold, then  $Y$  must also be a manifold.*

*Proof.* Observe that  $Y$  is homeomorphic to  $(X \times Y)/X$ , which is the quotient of two manifolds via the projection map, which is a surjective submersion. Hence  $Y$  is a manifold.  $\square$

Consequently, the contrapositive of Lemma 1 states that if  $T$  is not a manifold but  $T^{w-1}$  is a manifold, it follows that the space of sequences of tokens<sup>2</sup>  $T^w$  cannot be a manifold. At best, the latent space for every other context window size can be a manifold. For every proposed context window length, a longer window will exhibit singularities. In short, *lengthening the context window does not persistently resolve singularities* in the token embedding.

The remaining question is whether these singularities persist into the *output* of the LLM. Can the user elicit the instabilities caused by singularities? We provide sufficient conditions for unstable outputs:

**Theorem 2.** *Let  $Z$  be the  $d$ -dimensional bounding manifold<sup>3</sup> for the token subspace, such that  $T \subseteq Z$ . Consider an LLM with a context window of size  $w$ , in which the latent space of tokens is  $\mathbb{R}^\ell$ , and we collect  $m$  tokens as output from this LLM.*

*Suppose the following:*

- (1) *(enough tokens are collected from the response)  $m > \frac{2wd}{\ell}$ , but*
- (2) *(the context window is longer than the number of tokens we collected)  $w \geq m$ .*

*Under these conditions, a generic set of transformers yield a topological embedding of  $T^w$  into the output of the LLM.*

*Proof.* See Section A.4  $\square$

As a consequence, there always exists such an  $m$  satisfying the hypothesis if  $2d < \ell$ , i.e. the bounding manifold has dimension less than half the latent space dimension. If our hypothesis tests show that the token subspace contains singularities and the hypotheses of Theorem 2 are satisfied, singularities will persist into the output of the LLM for generic transformers even for large context window sizes.

**3.3. Experimental results.** We applied our test to the token subspaces of the four open source LLMs introduced in Sec. 4.1: GPT2, Llemma7B, Mistral7B, and Pythia6.9B. In each LLM we tested, we found evidence that *the token subspace is not globally a manifold because the local dimension is highly variable. Moreover, we can infer that they are either not fiber bundles or have high curvature locally*; in

---

<sup>2</sup>Caution:  $T^w$  is the sequence of tokens embedded *individually*, which is different from the embedding of the *entire sequence*. Theorem 2 asserts conditions under which  $T^w$  has a direct impact on LLM output.

<sup>3</sup>Since  $T \subseteq \mathbb{R}^\ell$ , it is always contained within such a bounding manifold  $Z \subseteq \mathbb{R}^\ell$ .

---

either case—violating the hypotheses or having high curvature—model behavior near certain tokens will be highly unstable.

We observe highly statistically significant differences in the irregular tokens *between* LLMs—even for those with identical sets of tokens overall—which indicates that their respective training methodologies have a strong impact on the token subspace. Given these differences, prompts containing irregular tokens will likely produce dissimilar outputs across the four LLMs corroborating the results shown by [17]. Additionally, prompts containing irregular tokens within an LLM will likely be unstable and produce highly variable outputs with replicated queries. This is clear if  $B(\psi)$  contains a singularity but will also be true for regions of high curvature resulting in instability for both interpolation and extrapolation tasks ([39]).

Several non-manifold features are visibly present in Figure 1. The tokens “ember” and “P” appear to be both putative examples of *cusp points*, places where the space exhibits a sharp exposed point. Manifolds cannot have cusp points, so attempting to approximate a cusp with a manifold—for instance, with UMAP—necessitates high curvature. The tokens “:” and “ly” appear to be *pinch points*—like what are present in a chain of sausages—which again cannot be approximated by a manifold unless it has high curvature.

Several additional views of Figure 1 are shown in Figure 6 in the Supplement. The coordinates, token text,  $p$ -values, and a video of the space with commentary are available in the ZIP file Supplement.

Table 1 shows the results of our hypothesis tests for the four models we analyzed. It is clear that the models have quite different token input embeddings, and all of them exhibit highly significant rejections of the manifold hypothesis. GPT2, Llemma7B and Mistral7B also reject the fiber bundle hypothesis. The rejections of the fiber bundle hypothesis are more frequent in the larger radius region than the smaller radius region, which is consistent with the polysemy interpretation of [22].

While most of the tokens are not shared between the LLMs, Llemma7B and Mistral7B do have identical token sets. The fact that Table 1 shows significant differences between these two models indicates that the structure of the irregularities for these two models is quite different. This implies that their response to the same prompt is expected to be markedly different, even without considering the differences in their respective transformer stages.

Since there are many rejections of the manifold hypothesis, we summarize some general trends.

- The GPT2 tokens at irregularities are tokens that can only appear at the beginning of words.
- The Pythia6.9B tokens at irregularities are nearly all word fragments or short sequences of text that are quite meaningless on their own.
- The Llemma7B and Mistral7B tokens at irregularities are a combination of the previous two: either they can only appear at the beginning of words or they are word fragments.

Estimates of the bounding manifold dimension used in Theorem 2 for the four LLMs we studied are in the “dimension” columns of Table 1, with the most stringent being the dimension for smaller radius. Table 2 shows the results of testing the hypotheses of Theorem 2 using the medians (Q2). Mistral7B, and Pythia6.9B satisfy the hypotheses of Theorem 2 using the small radius dimension estimates, but GPT2 and Llemma7B do not. All four LLMs satisfy the hypotheses of Theorem 2 if we

This material is based upon work supported by the Defense Advanced Research Projects Agency (DARPA) under Contract No. HR001124C0319. Any opinions, findings and conclusions or recommendations expressed in this material are those of the author(s) and do not necessarily reflect the views of the Defense Advanced Research Projects Agency (DARPA). Distribution Statement “A” (Approved for Public Release, Distribution Unlimited).

TABLE 1. Dimensional data for and number of tokens rejecting the manifold and fiber bundle hypotheses at two slope changes.  $n$  is the number of tokens (vocabulary size) in each model. The  $p$ -values displayed report the minimum  $p$ -value for each test, accounting for multiple testing. Quartiles (Q2 is the median) are shown for the distribution of the dimensions estimated from the slopes of the log-volume versus log-radius plots aggregated over all tokens. The “rejects” columns list the number of tokens rejecting each hypothesis. Table 3 (resp. Table 4–9) in the Supplementary material shows each of the fiber bundle (manifold hypothesis) violations for each model that is listed here.

Model	Manifold rejects	Fiber bundle			
		Smaller dim.	Radius rejects	Larger dim.	rejects
GPT2 $n = 50257$	68 $p \approx 3 \times 10^{-8}$	Q1: 20 Q2: 389 Q3: 531	12 $p \approx 9 \times 10^{-6}$	Q1: 8 Q2: 14 Q3: 32	7 $p \approx 3 \times 10^{-8}$
Llemma7B $n = 32016$	33 $p \approx 5 \times 10^{-9}$	Q1: 4096 Q2: 4096 Q3: 4096	0 N/A	Q1: 8 Q2: 11 Q3: 14	1 $p \approx 3 \times 10^{-4}$
Mistral7B $n = 32016$	40 $p \approx 3 \times 10^{-7}$	Q1: 9 Q2: 48 Q3: 220	1 $p \approx 8 \times 10^{-4}$	Q1: 5 Q2: 6 Q3: 9	2 $p \approx 8 \times 10^{-5}$
Pythia6.9B $n = 50254$	54 $p \approx 2 \times 10^{-7}$	Q1: 2 Q2: 108 Q3: 235	0 N/A	Q1: 2 Q2: 5 Q3: 145	0 N/A

TABLE 2. Testing the hypotheses of Theorem 2: Will singularities generically persist into the output? See statement of Theorem 2 for variable definitions. “Small” and “Large” refer to the small and large radius estimates of dimensions from Table 1.

Model	Latent dim $\ell$	Bounding dim. $d$		Context $w$	Min. output tokens $m$ such that		Satisfied? $w \geq m?$	
		Small	Large		Small	Large	Small	Large
GPT2	768	389	14	1024	1038	38	No	Yes
Llemma7B	4096	4096	11	4096	8193	23	No	Yes
Mistral7B	4096	48	6	4096	97	13	Yes	Yes
Pythia6.9B	4096	108	5	4096	217	11	Yes	Yes

instead use the larger radius dimension estimates. This means that it is likely that the transformers of Mistral7B, and Pythia6.9B are unable to resolve the singularities that we show exist in the token subspace, so singularities will persist in the output of the model. If the true bounding manifold for GPT2 or Llemma7B is smaller than the small radius estimate suggests, these too will likely produce singularities in their output.

This material is based upon work supported by the Defense Advanced Research Projects Agency (DARPA) under Contract No. HR001124C0319. Any opinions, findings and conclusions or recommendations expressed in this material are those of the author(s) and do not necessarily reflect the views of the Defense Advanced Research Projects Agency (DARPA). Distribution Statement “A” (Approved for Public Release, Distribution Unlimited).

---

#### 4. DISCUSSION

*None* of the four LLMs we studied are manifold globally given non-constant local dimension. Locally, the token subspace cannot be manifolds with large reach, and three of the four also cannot be fiber bundles with large reach. Irregularities—tokens that cause rejections of the manifold hypothesis—occur in different ways across all four LLMs. Additionally, irregularities corresponding to violations of the fiber bundle hypothesis are tokens whose neighborhoods exhibit a dependency between the large- and small-scale variability.

The grammatical role of tokens is likely a root cause for some of sensitivity of LLMs to their prompts that has been observed in the literature ([20, 21]), and may explain why “explaining LLM behavior” remains challenging and open. Most methods for explaining LLM behavior in terms of dynamical systems, for instance, derive their inferential power from assuming that the token subspace is a manifold ([40, 41, 42]). *Our results indicate that these theoretical methods may not apply to current LLMs.*

One might argue that context helps to disambiguate and “fix” these problems, but this intuitive argument seems not always possible as context alone is insufficient to resolve singularities. As we showed in Section 3.2, *singularities in the token subspace persistently lead to singularities in the space of token sequences, and under appropriate conditions these propagate into the output of an LLM.*

Irregularities—which may in fact be singularities—are noticeable in a PCA projection of the token subspace (Figure 1 and Figure 6). Intuitively, this means that the use of inner products to perform token de-embeddings by orthogonal projections may not be accomplishing the intended objectives. Even small perturbations within the latent space may result in instabilities in these projections, providing potential explanations for the instabilities in LLM outputs.

In addition to token instability, the fact that token subspaces are not manifolds and may have small reach means that the geodesic distance between tokens can also be very unstable. While the distance along geodesics can be defined, it may not correlate with any sense of semantic distance between tokens. Furthermore, as [38] found, in most of the models, there are tokens with dimension 0 neighborhoods. These tokens are theoretically *isolated*, implying that the token subspace is disconnected and hence intrinsically infinitely far from other tokens.

Singularities may arise either as artifacts of the training process or from features of the languages being represented. Consistent with the idea that polysemy may yield singularities ([22]), several of the tokens where the fiber bundle hypothesis is rejected are clear homonyms. For instance, both “affect” and “monitor” can be used as either nouns or verbs, and their meanings are different in these two roles. Tokens also form fragments of text, and so, a token may correspond to homonyms after the addition of a prefix or suffix. A token like “aunder” can be prefixed to yield the word “launder”, a word with multiple meanings of opposite sense. Specifically, one can “launder” clothing (positive connotation) or “launder” money (negative connotation). Several other tokens where the fiber bundle hypothesis is violated form words with substantially different meanings or grammatical roles upon adding a prefix or suffix. For instance, “wins” can function as a noun, as a verb, or form the adjective “winsome”.

The differences in how the manifold and fiber bundle hypotheses are rejected across different LLMs suggest that the training methodology for each model leaves

This material is based upon work supported by the Defense Advanced Research Projects Agency (DARPA) under Contract No. HR001124C0319. Any opinions, findings and conclusions or recommendations expressed in this material are those of the author(s) and do not necessarily reflect the views of the Defense Advanced Research Projects Agency (DARPA). Distribution Statement “A” (Approved for Public Release, Distribution Unlimited).

---

an indelible fingerprint (or gDNA coined by [17]). Making general assertions about LLMs without consideration of their training and evolution is likely fraught. Even between Llemma7B and Mistral7B, which have identical token sets, *prompts likely cannot be “ported” from one LLM to another without significant modifications if they contain tokens near irregularities*. This may have serious ramifications for interacting LLMs such as those powering multi-agentic frameworks being deployed today ([43, 44, 45]).

A few clear patterns among tokens near irregularities are nevertheless noticeable. Tokens that begin a word or are a word fragment are often located at an irregularity. Additionally, in Llemma7B (but not Mistral7B) and Pythia6.9B the tokens with unusually low fiber dimension often contain non-printing or whitespace characters. This suggests that these models are quite sensitive to text layout, perhaps to the exclusion of more semantically salient features in the text. Given our findings, future experiments can be run to explore the impact of irregular tokens on the variability of responses produced by different LLMs.

As we attempt to model natural phenomena particularly in our physical world, we know singularities exist (e.g. phase transitions), and so assuming regularity limits our understanding of the natural world. Our work extends this notion to the linguistics of natural language where its richness and complexity do not appear to manifest in a smooth representation.

**4.1. Limitations.** While topological theory motivates our statistical test, only the slope changes that occur for radii less than the embedded reach correspond to rejections of the manifold or fiber bundle hypotheses. If the reach of a manifold is small, then it likely has a high local curvature, and measuring distances on that surface will be numerically unstable. As a result, the reach itself is difficult to estimate accurately from sampled data ([23, 46, 47]). Our implementation tests the radius below an estimated reach, determined by an inspection of the radius-vs-volume plots of a random sample of tokens. If the true reach is smaller than our estimates, the curvature of the manifolds that fit the data well, found by *any* method, will be high.

And lastly, we emphasize that these tests allow us to reject the structure assumed in our null hypothesis (smooth and regular), but do not permit us to infer an alternative. While rejecting regularity does imply singularity, it does not afford us any evidence as to the type of singularity. That must be determined *post hoc* if possible.

#### ACKNOWLEDGMENTS

The authors would like to thank Mohammed Abouzaid, Anand Sarwate, Andrew Lauziere, and Andrew Engel for helpful suggestions on a draft of this manuscript.

This material is based upon work partially supported by the Defense Advanced Research Projects Agency (DARPA) under Contract No. HR001124C0319. Any opinions, findings and conclusions or recommendations expressed in this material are those of the author(s) and do not necessarily reflect the views of the Defense Advanced Research Projects Agency (DARPA). Distribution Statement “A” (Approved for Public Release, Distribution Unlimited) applies to the portion of the work funded by DARPA.

This material is based upon work supported by the Defense Advanced Research Projects Agency (DARPA) under Contract No. HR001124C0319. Any opinions, findings and conclusions or recommendations expressed in this material are those of the author(s) and do not necessarily reflect the views of the Defense Advanced Research Projects Agency (DARPA). Distribution Statement “A” (Approved for Public Release, Distribution Unlimited).

---

## REFERENCES

- [1] David Gunning, Mark Stefik, Jaesik Choi, Timothy Miller, Simone Stumpf, and Guang-Zhong Yang. XAI—Explainable artificial intelligence. *Science Robotics*, 4(37):eaay7120, 2019.
- [2] Colin S. Gordon. The linguistics of programming. In *SIGPLAN symposium on New ideas, new paradigms, and reflections on programming and software*, 2024.
- [3] Zhaofeng Wu, William Merrill, Hao Peng, Iz Beltagy, and Noah A. Smith. Transparency helps reveal when language models learn meaning. *Transactions of the Association for Computational Linguistics*, 11:617–634, 2022.
- [4] Aaron Traylor, Roman Feiman, and Ellie Pavlick. And does not mean or: Using formal languages to study language models’ representations. In *Annual Meeting of the Association for Computational Linguistics*, 2021.
- [5] Zhiqian Tan, Chenghai Li, and Weiran Huang. The information of large language model geometry. *ArXiv*, abs/2402.03471, 2024.
- [6] Xuhong Wang, Haoyu Jiang, Yi Yu, Jingru Yu, Yilun Lin, Ping Yi, Yingchun Wang, Yu Qiao, Li Li, and Fei-Yue Wang. Building intelligence identification system via large language model watermarking: A survey and beyond. *ArXiv*, abs/2407.11100, 2024.
- [7] Shi Chen, Zhengjiang Lin, Yury Polyanskiy, and Philippe Rigollet. Quantitative clustering in mean-field transformer models. *arXiv preprint arXiv:2504.14697*, 2025.
- [8] Borjan Geshkovski, Cyril Letrouit, Yury Polyanskiy, and Philippe Rigollet. A mathematical perspective on transformers. *ArXiv*, abs/2312.10794, 2023.
- [9] Yiping Lu, Zhuohan Li, Di He, Zhiqing Sun, Bin Dong, Tao Qin, Liwei Wang, and Tie-Yan Liu. Understanding and improving transformer from a multi-particle dynamic system point of view. *ArXiv*, abs/1906.02762, 2019.
- [10] Yi-Chong Huang, Xiaocheng Feng, Baohang Li, Yang Xiang, Hui Wang, Bing Qin, and Ting Liu. Ensemble learning for heterogeneous large language models with deep parallel collaboration. In *Neural Information Processing Systems*, 2024.
- [11] Nicholas M. Asher, Swarnadeep Bhar, Akshay Chaturvedi, Julie Hunter, and Soumya Paul. Limits for learning with language models. *ArXiv*, abs/2306.12213, 2023.
- [12] Tai-Danae Bradley and Juan Pablo Vigneaux. The magnitude of categories of texts enriched by language models, 2025.
- [13] Archit Rathore, Yichu Zhou, Vivek Srikumar, and Bei Wang. Topobert: Exploring the topology of fine-tuned word representations. *Information Visualization*, 22(3):186–208, 2023.
- [14] Tai-Danae Bradley, John Terilla, and Yiannis Vlassopoulos. An enriched category theory of language: from syntax to semantics. *La Matematica*, 1(2):551–580, 2022.
- [15] Mudit Verma, Siddhant Bhambri, and Subbarao Kambhampati. On the brittle foundations of react prompting for agentic large language models. *ArXiv*, abs/2405.13966, 2024.
- [16] Jia He, Mukund Rungta, David Koleczek, Arshdeep Sekhon, Franklin X Wang, and Sadid A. Hasan. Does prompt formatting have any impact on llm performance? *ArXiv*, abs/2411.10541, 2024.
- [17] Max Vargas, Reilly Cannon, Andrew Engel, Anand D Sarwate, and Tony Chiang. Understanding generative ai content with embedding models, 2024.
- [18] Yuxi Li, Yi Liu, Gelei Deng, Ying Zhang, Wenjia Song, Ling Shi, Kailong Wang, Yuekang Li, Yang Liu, and Haoyu Wang. Glitch tokens in large language models: Categorization taxonomy and effective detection. *Proc. ACM Softw. Eng.*, 1:2075–2097, 2024.
- [19] Karthik Valmeekam, Matthew Marquez, Sarah Sreedharan, and Subbarao Kambhampati. On the planning abilities of large language models - a critical investigation. *ArXiv*, abs/2305.15771, 2023.
- [20] Melanie Sclar, Yejin Choi, Yulia Tsvetkov, and Alane Suhr. Quantifying language models’ sensitivity to spurious features in prompt design or: How I learned to start worrying about prompt formatting. *ArXiv*, abs/2310.11324, 2023.
- [21] Patrick Chao, Alexander Robey, Edgar Dobriban, Hamed Hassani, George J Pappas, and Eric Wong. Jailbreaking black box large language models in twenty queries. *arXiv preprint arXiv:2310.08419*, 2023.
- [22] Alexander Jakubowski, Milica Gasic, and Marcus Zibrowius. Topology of word embeddings: Singularities reflect polysemy. In Iryna Gurevych, Marianna Apidianaki, and Manaal Faruqui, editors, *Proceedings of the Ninth Joint Conference on Lexical and Computational Semantics*,

---

pages 103–113, Barcelona, Spain (Online), December 2020. Association for Computational Linguistics.

[23] C. Berenfeld, J. Harvey, M. Hoffmann, and K. Shankar. Estimating the reach of a manifold via its convexity defect function. *Discrete and computational geometry*, pages 403–438, 2022.

[24] Alec Radford, Jeffrey Wu, Rewon Child, David Luan, Dario Amodei, Ilya Sutskever, et al. Language models are unsupervised multitask learners. *OpenAI blog*, 1(8):9, 2019.

[25] Zhangir Azerbayev, Hailey Schoelkopf, Keiran Paster, Marco Dos Santos, Stephen McAleer, Albert Q. Jiang, Jia Deng, Stella Biderman, and Sean Welleck. Llemma: An open language model for mathematics, 2024.

[26] Albert Q. Jiang, Alexandre Sablayrolles, Arthur Mensch, Chris Bamford, Devendra Singh Chaplot, Diego de las Casas, Florian Bressand, Gianna Lengyel, Guillaume Lample, Lucile Saulnier, Lélio Renard Lavaud, Marie-Anne Lachaux, Pierre Stock, Teven Le Scao, Thibaut Lavril, Thomas Wang, Timothée Lacroix, and William El Sayed. Mistral7b, 2023.

[27] Stella Biderman, Hailey Schoelkopf, Quentin Anthony, Herbie Bradley, Kyle O'Brien, Eric Hallahan, Mohammad Aflah Khan, Shivanush Purohit, USVSN Sai Prashanth, Edward Raff, Aviya Skowron, Lintang Sutawika, and Oskar van der Wal. Pythia: A suite for analyzing large language models across training and scaling, 2023.

[28] Minsu Park, Marco Gatti, and Bhuvnesh Jain. Dimensionality reduction techniques for statistical inference in cosmology. *Physical Review D*, 2024.

[29] T. Lucas Makinen, Alan Heavens, Natalia Porqueres, Tom Charnock, Axel Lapel, and Benjamin D. Wandelt. Hybrid summary statistics: neural weak lensing inference beyond the power spectrum. *ArXiv*, abs/2407.18909, 2024.

[30] Lucas Einig, J'erome Pety Iram, Lerma, Antoine Roueff, Pauline Vandame, Jocelyn Chanussot, Maryvonne Gerin, Jan H. Orkisz, Pierre Palud, M. Santa-Maria, Victor de Souza Magalhaes, Ivana Bevsl'i'c, Sébastien Bardeau, Emeric Bron, Pierre Chainais, Javier R. Goicoechea, Pierre Gratier, Viviana Guzman Veloso, Annie Hughes, Jouni Kainulainen, David Languignon, Rosine Lallement, Francois Levrier, Dariusz C. Lis, Harvey S. Liszt, Jacques Le Bourlot, Franck Le Petit, Karin Danielsson Oberg, Nicolas Peretto, Evelyne Roueff, Albrecht Sievers, Pierre-Antoine Thouvenin, and Pascal Tremblin. Deep learning denoising by dimension reduction: Application to the orion-b line cubes. *Astronomy & Astrophysics*, 2023.

[31] Naoki Masuda and Prosenjit Kundu. Dimension reduction of dynamical systems on networks with leading and non-leading eigenvectors of adjacency matrices. *Physical Review Research*, 2022.

[32] Todd L. Parsons and Tim Rogers. Dimension reduction via timescale separation in stochastic dynamical systems. *arXiv: Probability*, 2015.

[33] Bahram Hemmateenejad, Mohammad A. Safarpour, Ramin Miri, and Fariba Taghavi. Application of ab initio theory to qsar study of 1,4-dihydropyridine-based calcium channel blockers using ga-mlr and pc-ga-ann procedures. *Journal of Computational Chemistry*, 25, 2004.

[34] Leland McInnes, John Healy, and James Melville. Umap: Uniform manifold approximation and projection for dimension reduction. *arXiv preprint arXiv:1802.03426*, 2018.

[35] Charles Fefferman, Sanjoy Mitter, and Hariharan Narayanan. Testing the manifold hypothesis. *Journal of the American Mathematical Society*, 29(4):983–1049, 2016.

[36] Vasilii A. Gromov, Nikita S. Borodin, and Asel S. Yerbolova. A language and its dimensions: Intrinsic dimensions of language fractal structures. *Complexity*, 2024.

[37] Eduard Tulchinskii, Kristian Kuznetsov, Laida Kushnareva, Daniil Cherniavskii, Serguei Barannikov, Irina Piontkovskaya, Sergey Nikolenko, and Evgeny Burnaev. Intrinsic dimension estimation for robust detection of AI-generated texts, 2023.

[38] Michael Robinson, Sourya Dey, and Shauna Sweet. The structure of the token space for large language models, 2024.

[39] Eugene Isaacson and Herbert Bishop Keller. *Analysis of numerical methods*. Courier Corporation, 2012.

[40] Toni JB Liu, Nicolas Boullié, Raphaël Sarfati, and Christopher J Earls. Llms learn governing principles of dynamical systems, revealing an in-context neural scaling law. *arXiv preprint arXiv:2402.00795*, 2024.

[41] Pratik Prabhanjan Brahma, Dapeng Wu, and Yiyuan She. Why deep learning works: A manifold disentanglement perspective. *IEEE transactions on neural networks and learning systems*, 27(10):1997–2008, 2015.

---

- [42] Hariharan Narayanan and Sanjoy Mitter. Sample complexity of testing the manifold hypothesis. *Advances in neural information processing systems*, 23, 2010.
- [43] WenYuan Gu, JiaLe Han, HaoWen Wang, Xiang Li, and Bo Cheng. Explain-analyze-generate: A sequential multi-agent collaboration method for complex reasoning. In Owen Rambow, Leo Wanner, Marianna Apidianaki, Hend Al-Khalifa, Barbara Di Eugenio, and Steven Schockaert, editors, *Proceedings of the 31st International Conference on Computational Linguistics*, pages 7127–7140, Abu Dhabi, UAE, January 2025. Association for Computational Linguistics.
- [44] Can Jin, Hongwu Peng, Qixin Zhang, Yujin Tang, Dimitris N. Metaxas, and Tong Che. Two heads are better than one: Test-time scaling of multi-agent collaborative reasoning, 2025.
- [45] Chen Qian, Zihao Xie, YiFei Wang, Wei Liu, Kunlun Zhu, Hanchen Xia, Yufan Dang, Zhuoyun Du, Weize Chen, Cheng Yang, Zhiyuan Liu, and Maosong Sun. Scaling large language model-based multi-agent collaboration, 2025.
- [46] Michael Rawson and Michael Robinson. Instability of manifold reach and a stable combinatorial reach. In *Online International Conference on Computational Harmonic Analysis*, 2021.
- [47] Eddie Aamari and Clément Levraud. Nonasymptotic rates for manifold, tangent space and curvature estimation. *Ann. Statist.*, 47(1):177–204, 2019.
- [48] J. Lee. *Smooth Manifolds*. Springer, 2003.
- [49] Alfred Gray. The volume of a small geodesic ball of a Riemannian manifold. *Michigan Mathematical Journal*, 20(4):329 – 344, 1974.
- [50] Michael Robinson, Sourya Dey, and Taisa Kushner. Probing the topology of the space of tokens with structured prompts, 2025.

---

## APPENDIX A. SUPPLEMENTARY MATERIAL

**A.1. Background.** At an abstract but precise level, an LLM consists of several interacting processes, as outlined in Figure 4. An LLM implements a transformation of a sequence of tokens (the query) into a new sequence of tokens (the response). Formally, if each input token is an element of a metric space  $T$ , then the LLM is a transformation  $T^w \rightarrow T^m$ , where  $w$  is the number of tokens in the query and  $m$  is the number of tokens in the response. This transformation is typically *not* a function because it is stochastic—it involves random draws.

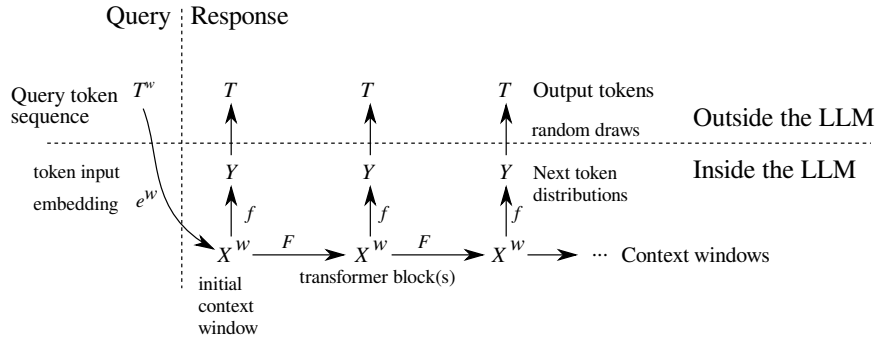


FIGURE 4. Data flow in a typical LLM. A sequence of tokens forming the query is converted via the token input embedding  $e^w$  into the initial context window, as a point in the latent space  $X^w$ . Each of these windows in the latent space are converted, token-by-token, into probability distributions via  $f$  into the single token latent space  $X$ . From these, each token presented in the output (in the set  $Y$ ) is obtained via a random draw. These output tokens are then used for subsequent windows.

To operate upon tokens using numerical models, such as could be implemented using neural networks, we must transform the finite set of tokens  $T$  into numerical data. This is typically done by way of a pair of *latent spaces*  $X = \mathbb{R}^\ell$  and  $Y = \mathbb{R}^q$ . The dimension  $q$  of  $Y$  is chosen to be equal to the number of elements in  $T$ , so that elements of  $Y$  have the interpretation of being (unnormalized) probability distributions over  $T$ .

The transformation  $T^w \rightarrow T^m$  is constructed in several stages.

**Input tokenization:** : Each token is embedded individually via the *token input embedding* function  $e : T \rightarrow X$ . As a whole,  $X^w$  is called a *latent window*.

**Transformer blocks:** : The probability distribution for the next token is constructed by a continuous function  $f : X^w \rightarrow Y$ . This is usually implemented by one or more *transformer blocks*.

**Output tokenization:** : Given the output of one of the transformer blocks  $f$ , one can obtain an output token in  $T$  by a random draw. Specifically, if  $(\psi_1, \psi_2, \dots, \psi_w)$  is the current window in  $X^w$ , then the next token  $t$  is drawn from the distribution given by  $f(\psi_1, \psi_2, \dots, \psi_w)$ .

**Next window prediction:** : Given that token  $t$  was drawn from the distribution, the next latent window itself is constructed by a transformation

---

$F : X^w \rightarrow X^w$ , which advances the window as follows:

$$F(\psi_1, \psi_2, \dots, \psi_w) := (\psi_2, \dots, \psi_w, t).$$

Note well: the function  $e^w : T^w \rightarrow X^w$  which transforms a sequence of individual tokens into coordinates in the latent space is merely the first stage in the process. As such,  $e^w$  is *distinct from* the embedding of sequences provided by many LLM software interfaces. That sequence embedding is properly an intermediate stage within the function  $f$ .

The focus of this paper is specifically upon the structure of the *token input embedding*  $e : T \rightarrow X = \mathbb{R}^\ell$ . Since the token set  $T$  is finite,  $e$  can be stored as a matrix. In this matrix, each column corresponds to an element of  $T$ , and thereby ascribes a vector of numerical coordinates to each token. By replacing the last layer of the deep neural network  $f : X^w \rightarrow Y$ , a vector of probabilities for the next token is obtained from the activations of the last layer. One can therefore interpret the probabilities as specifying a *token output embedding*. Both the tokenization and the transformer stages are learned during training, and many strategies for this learning process are discussed extensively in the literature. These two stages interact when they produce the LLM output, so it is important to understand the lineage of a given tokenization as being from a particular LLM.

**A.2. Computational resource requirements.** Applying our entire method (starting with the token embedding matrix and ending with the  $p$ -values for each of the three tests at every token) to each model took approximately 12 hours of wall clock time (per model) on an Intel Core i7-3820 with 32 GB of CPU RAM and no GPU running at 3.60GHz. Almost all of the runtime was spent computing the token distance matrix. The subsequent stages, including the three hypothesis tests, shown in Figure 2 run in only a few minutes on the same machine. The distance matrix calculation was performed using `scipy.spatial.distance_matrix()`, which produces a dense matrix, by computing the distance between all pairs of tokens in the latent space. Because of the relatively low runtime requirements, we did not feel the need to use sparsity-enhancing techniques to accelerate the distance matrix calculation.

**A.3. Interpretation of fiber bundles in terms of spatial variability.** It is usual to describe measurements as exhibiting the combined effect of multiple spatial scales. One way this might arise is if we could express each measurement as being an ordered pair (signal, noise), with the short spatial scales correlating to noise and the longer spatial scales correlating to the signal. With this interpretation, if the space of all possible signals is  $S$  and the space of all noise values is  $V$ , we could represent the space of all possible measurements as the cartesian product  $E = S \times V$ . This cartesian product representation can arise for noiseless data as well, as it merely captures multiple spatial scales. In what follows, we will call  $S$  the *base space* and  $V$  the *fiber space*.

Figure 5 shows an example of this situation. It consists of a 1-dimensional base space (the long spatial scale) and 1-dimensional fibers (the short spatial scale), which in this case forms a narrow strip in the plane. Volumes (areas, in this case) of balls of small radius scale quadratically (slope 2 in a log-log plot), but scale asymptotically linearly (slope 1 in a log-log plot) for large radii. The transition between these two behaviors is detectable by way of a corner in the plot. This

This material is based upon work supported by the Defense Advanced Research Projects Agency (DARPA) under Contract No. HR001124C0319. Any opinions, findings and conclusions or recommendations expressed in this material are those of the author(s) and do not necessarily reflect the views of the Defense Advanced Research Projects Agency (DARPA). Distribution Statement “A” (Approved for Public Release, Distribution Unlimited).

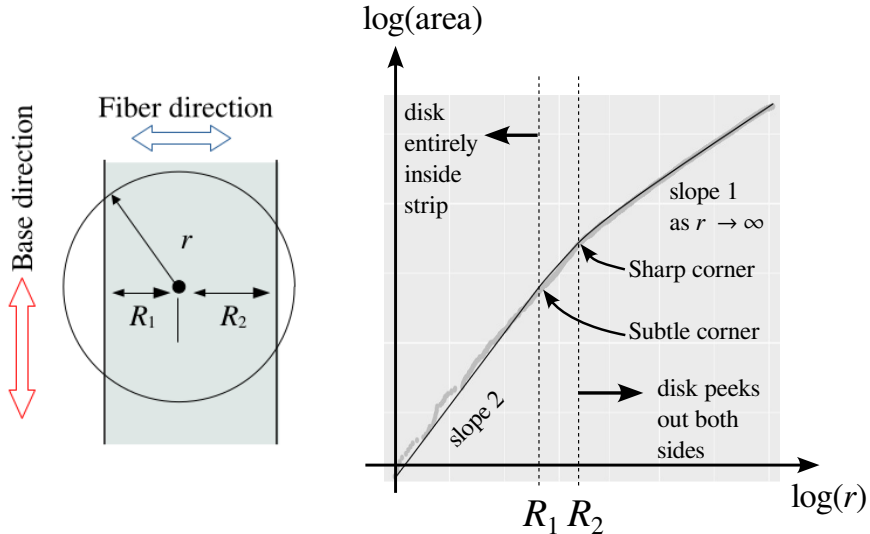


FIGURE 5. Our method applied to a fiber bundle in  $\mathbb{R}^2$ . The vertical direction is the base space (long spatial scale), while the horizontal direction represents the fibers space (short spatial scale). Gray points on the right frame show estimates from a random sampling of points in the strip; the solid line shows the theoretical area versus radius curve.

situation is easily and robustly estimated from the data; the gray points in Figure 5 (right) are derived from a random sampling of points drawn from the strip.

To test for multiple spatial scales, we propose a signal model that is mathematically represented by a *fiber bundle*. In a fiber bundle, the long spatial scales are modeled by a space  $S$ , but all possible measurements are modeled by a function  $p : E \rightarrow S$ . The idea is that *fibers*  $p^{-1}(b)$  are still cartesian products: pairs of both spatial scales, and these are all identical up to *diffeomorphism*. Our method relies upon a particular geometric property of fiber bundles: we can identify if the fibers are not all identical according to when the conclusion of Theorem 1 is violated.

One possible way that a fiber bundle might arise is if the underlying noise model is *homooscedastic*, which is to say that the dimensionality of the noise near a token does not depend on that token. In this case, the fibers (short spatial scales) mostly correspond to noise, and the base (long spatial scales) correspond mostly to signal. Nevertheless, a fiber bundle may arise with noiseless data as well; the presence of multiple spatial scales is what matters.

On the other hand, if the underlying noise model is *heteroscedastic*—it depends on the token in question—then the fiber bundle model should be rejected. Figure 3(a) shows a situation that is not a fiber bundle, since there is a change in the dimension of the fiber. In the upper portion of the figure, the fiber dimension is 0 while in the lower portion the fiber dimension is 1. This is detectable by looking at the volume versus radius plots for two samples. While both samples show corners in their volume versus radius plots, Theorem 1 establishes that *the slopes always decrease with increasing radius* for a fiber bundle. This is violated for the sample

---

marked  $\psi_1$ , so we conclude that the space is not a fiber bundle. On the other hand, because the sample marked  $\psi_2$  does not exhibit this violation, it is important to note that if a sample yields data consistent with Theorem 1, *we cannot* conclude that the space is a fiber bundle.

**A.4. Mathematical proof of Theorems 1 and 2.** This section contains mathematical justification for the fiber bundle hypothesis proposed earlier in the paper and the proof of Theorems 1 and 2. The central idea is the use of a special kind of fiber bundle, namely a fibered manifold with boundary.

By the submersion theorem ([48]), if the Jacobian matrix of a fibered manifold  $p : T \rightarrow S$  at every point has rank equal to the dimension of  $S$ , then the preimages  $p^{-1}(\psi) \subseteq T$  of each point  $\psi \in S$  are all diffeomorphic to each other. These preimages form the *fibers* discussed in the earlier sections of the paper.

As a consequence, each point  $y$  in the base space  $S$  has an open neighborhood  $U$  where the preimage  $p^{-1}(U)$  is diffeomorphic to the product  $U \times p^{-1}(y)$ , which is precisely the base-fiber split discussed in Section A.3. Specifically, the base dimension is simply the dimension of  $S$ , whereas the fiber dimension is the  $(\dim T - \dim S)$ .

The notion of a fibered manifold  $p : T \rightarrow S$  forms the intrinsic model of the data, which is only implicit in an LLM. The tokens present in a given LLM can be thought of as a sample from a probability distribution  $v$  on  $T$ , which can be taken to be the Riemannian volume form on  $T$  normalized so that  $v(T) = 1$ .

**Definition 2.** If  $e : T \rightarrow \mathbb{R}^\ell$  is a continuous map and  $v$  is a volume form on  $T$ , then the *pushforward* is defined by

$$(e_* v)(V) := v(e^{-1}(V))$$

for each measurable set  $V$ .

It is a standard fact that if  $e$  is a fibered manifold or an embedding, then  $e_* v$  is also a volume form.

*Proof.* (of Theorem 1) If  $e$  is assumed to be a smooth embedding<sup>4</sup>, the image of  $e$  is a manifold of dimension  $\dim T$ . The pushforward of a volume form is a contravariant functor, so this means that  $e_* v$  is the volume form for a Riemannian metric on  $e(T)$ . Using this Riemannian metric on  $e(T)$ , then [49, Thm 3.1] implies that for every  $\psi \in e(T)$ , if  $r \ll \tau$ , then

$$(2) \quad (e_* v)(B_r(\psi)) = O(r^{\dim T}).$$

Since  $T$  is compact,  $S$  is also compact via the surjectivity of  $p$ . This implies that there is a maximum radius  $r_1$  for which a ball of this radius centered on a point on  $\psi \in e(T)$  is entirely contained within  $e(T)$ . Also by compactness of  $S$ , there is a minimum radius  $r_2$  such that a ball of radius  $r_2$  centered on a point  $\psi \in e(T)$  contains a point outside of  $e(T)$ .

Since  $e$  is assumed to be an embedding, by the tubular neighborhood theorem ([48]), it must be that  $r_2 < \tau$ . Define

$$\rho(\psi) := \operatorname{argmax}_r \{B_r(\psi) \subseteq e(T)\},$$

from which it follows that  $0 < r_1 \leq \rho(\psi) \leq r_2 < \tau$ . As a result, Equation (2) holds for all  $r \leq \rho(\psi)$ , which is also the first case listed in Equation (1).

---

<sup>4</sup>Smoothness is not a strong constraint here. Any continuous function (such as ReLU) can be approximated well enough by a smooth map.

---

If  $r$  is chosen such that  $\rho(\psi) < r < \tau$ , the volume of the ball centered on  $\psi$  of radius  $r$  will be less than what is given by Equation (2), namely

$$(e_*v)(B_r(\psi)) < O(r^{\dim T}).$$

Since  $v$  is a volume form, its pushforward  $(p_*v)$  onto  $S$  is also a volume form. Moreover, via the surjectivity of  $p$ ,

$$\begin{aligned} (e_*v)(B_r(\psi)) &= v(e^{-1}(B_r(\psi))) \\ &\leq v(p^{-1}(p(e^{-1}(B_r(\psi))))) \\ &\leq (p_*v)(p(e^{-1}(B_r(\psi)))) \\ &\leq O(r^{\dim S}). \end{aligned}$$

From this, the second case of Equation (1) follows by recentering the asymptotic series on  $\rho(\psi)$ .  $\square$

Notice that the second case in Equation (1) may be precluded since while it holds for small  $r$ , it may be that  $\rho(\psi)$  may not be sufficiently small. As a consequence, the second case only occurs when both  $r$  and  $\rho(\psi)$  are sufficiently small. In the results shown in Section 3.3, both cases appear to hold frequently.

We now address Theorem 2.

*Proof.* (of Theorem 2) We need to manipulate the inequalities in the hypothesis to show that they satisfy [50, Thm. 1]. Once the hypothesis is satisfied, [50, Thm. 1] establishes that a generic set of transformers will embed  $T^w$  into the output of the LLM. Notice that [50, Thm. 1] considers the response of the LLM to a single token, though this can be easily extended by enlarging the bounding manifold dimension. With this in mind, the hypothesis to be satisfied is that

$$2wd < m\ell \leq wl.$$

The right inequality is clearly satisfied if context window is longer than number of output tokens collected, namely  $w \geq m$ . The left inequality is satisfied if

$$2d < \frac{m}{w}\ell,$$

which can be easily rearranged to the form in the hypothesis.  $\square$

**A.5. Additional views for Figure 1.** See Fig. 6.

**A.6. Table of fiber bundle rejections in all four LLMs.** See Table 3.

**A.7. Tables of manifold rejections in all four LLMs.** See Tables 4–9.

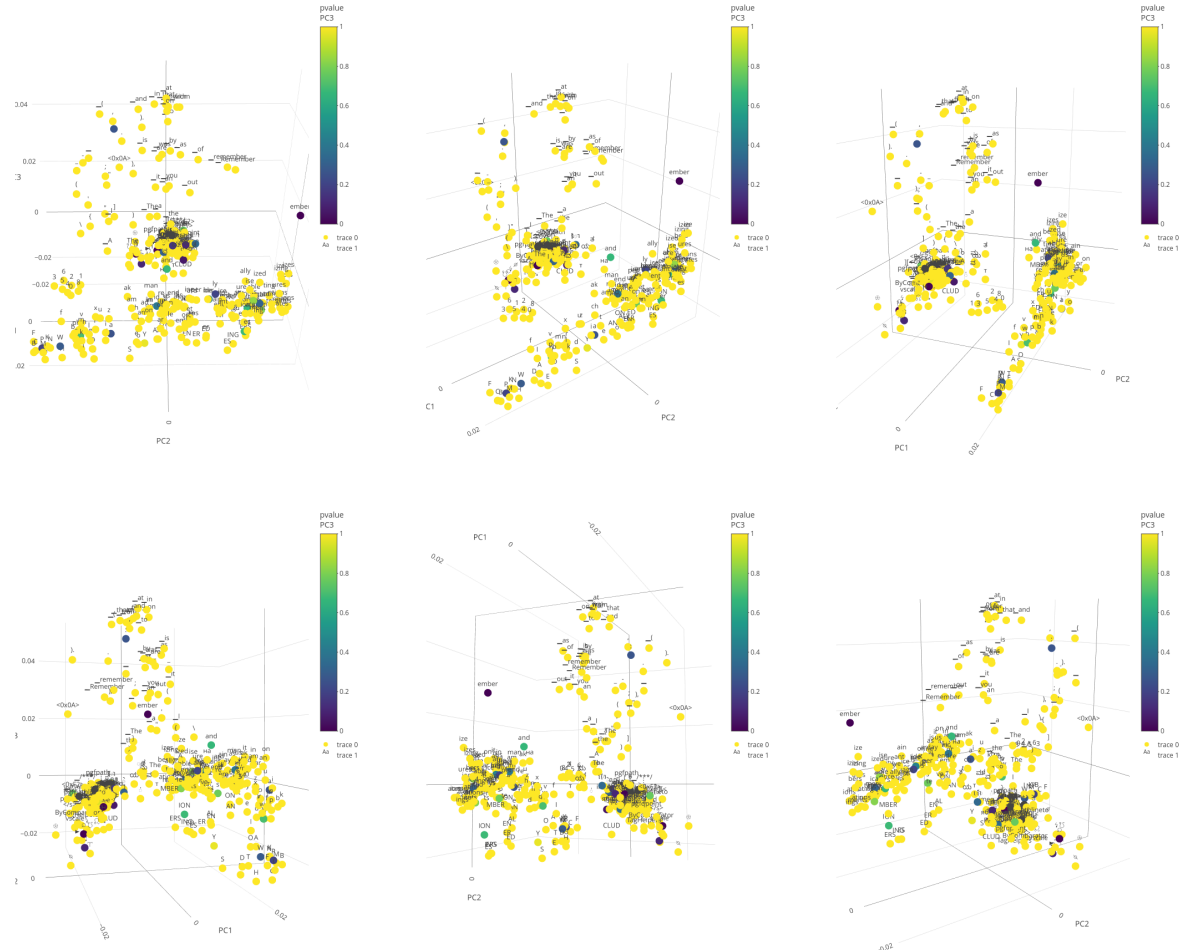


FIGURE 6. Additional rotational views of the PCA of the neighborhood of *ember* in Mistral7B shown in Figure 1. Each point shown is a token. Colors are *p*-values for the manifold hypothesis, with darker colors corresponding to lower likelihood that that point's neighborhood is a manifold with low curvature.

---

 TABLE 3. Violations of the fiber bundle hypothesis

Model	Token	Slope change	<i>p</i> -value	Comment
GPT2	<code>laughable</code>	Smaller radius	$9 \times 10^{-6}$	Must start a word
GPT2	<code>nuance</code>	Smaller radius	$2 \times 10^{-4}$	Must start a word
GPT2	<code>dt</code>	Smaller radius	$2 \times 10^{-4}$	
GPT2	<code>Mesh</code>	Smaller radius	$2 \times 10^{-4}$	
GPT2	<code>affect</code>	Smaller radius	$3 \times 10^{-4}$	Must start a word
GPT2	<code>Thankfully</code>	Smaller radius	$3 \times 10^{-4}$	
GPT2	<code>swat</code>	Smaller radius	$6 \times 10^{-4}$	Must start a word
GPT2	<code>Malaysian</code>	Smaller radius	$6 \times 10^{-4}$	Must start a word
GPT2	<code>Palestinian</code>	Smaller radius	$7 \times 10^{-4}$	Must start a word
GPT2	<code>wins</code>	Smaller radius	$8 \times 10^{-4}$	Must start a word
GPT2	<code>hedon</code>	Smaller radius	$9 \times 10^{-4}$	
GPT2	<code>donor</code>	Smaller radius	$9 \times 10^{-4}$	Must start a word
GPT2	<code>Xan</code>	Larger radius	$3 \times 10^{-8}$	Must start a word
GPT2	<code>aunder</code>	Larger radius	$2 \times 10^{-4}$	
GPT2	<code>Dri</code>	Larger radius	$2 \times 10^{-4}$	
GPT2	<code>ney</code>	Larger radius	$3 \times 10^{-4}$	
GPT2	<code>rodu</code>	Larger radius	$3 \times 10^{-4}$	
GPT2	<code>Insert</code>	Larger radius	$4 \times 10^{-4}$	
GPT2	<code>Ying</code>	Larger radius	$4 \times 10^{-4}$	Must start a word
Llemma7B	<code>pax</code>	Larger radius	$3 \times 10^{-4}$	
Mistral7B	<code>änge</code>	Smaller radius	$8 \times 10^{-4}$	
Mistral7B	<code>H0</code>	Larger radius	$5 \times 10^{-4}$	
Mistral7B	<code>monitor</code>	Larger radius	$8 \times 10^{-5}$	Must start a word

---

TABLE 4. Rejections of the manifold hypothesis for GPT2 (1 of 2)

Number	Token	<i>p</i> -value	Comment
1	Xan	0.0000000280	Must start a word
2	chemist	0.0000000602	
3	fry	0.00000564	Must start a word
4	laughable	0.00000807	Must start a word
5	Retro	0.0000108	Must start a word
6	laughable	0.0000156	Must start a word
7	Thankfully	0.0000339	
8	intoler	0.0000514	Must start a word
9	assumes	0.0000533	Must start a word
10	handwritten	0.0000783	Must start a word
11	MY	0.0000811	Must start a word
12	nuance	0.000105	Must start a word
13	playground	0.000110	Must start a word
14	dt	0.000124	
15	aunder	0.000132	
16	Mesh	0.000135	
17	Disney	0.000139	
18	McCl	0.000155	Must start a word
19	Dri	0.000196	
20	Destiny	0.000206	Must start a word
21	ney	0.000206	
22	juvenile	0.000209	Must start a word
23	advent	0.000211	Must start a word
24	perpet	0.000213	Must start a word
25	otally	0.000223	
26	affect	0.000226	Must start a word
27	efficient	0.000238	
28	rodu	0.000242	
29	Kl	0.000260	Must start a word
30	Thankfully	0.000278	
31	duct	0.000284	
32	frail	0.000292	Must start a word
33	alle	0.000304	Must start a word
34	Cha	0.000322	Must start a word
35	OO	0.000333	

---

TABLE 5. Rejections of the manifold hypothesis for GPT2 (2 of 2)

Number	Token	<i>p</i> -value	Comment
36	Insert	0.000336	
37	Ying	0.000357	Must start a word
38	Georgia	0.000373	
39	flo	0.000384	
40	uddled	0.000413	
41	subsequ	0.000421	Must start a word
42	lig	0.000439	Must start a word
43	Environmental	0.000456	Must start a word
44	Vladimir	0.000466	Must start a word
45	Defence	0.000510	Must start a word
46	swat	0.000558	Must start a word
47	registering	0.000564	Must start a word
48	Malaysian	0.000569	Must start a word
49	trough	0.000575	Must start a word
50	ears	0.000615	Must start a word
51	Meh	0.000637	Must start a word
52	Palestinian	0.000648	Must start a word
53	reckless	0.000654	Must start a word
54	Wax	0.000658	Must start a word
55	Dist	0.000673	Must start a word
56	Quad	0.000725	Must start a word
57	relations	0.000749	
58	wins	0.000781	Must start a word
59	KER	0.000785	
60	gist	0.000786	Must start a word
61	hedon	0.000834	
62	MMA	0.000839	Must start a word
63	donor	0.000865	Must start a word
64	aleb	0.000873	
65	Asked	0.000873	
66	Isaiah	0.000940	Must start a word
67	Survey	0.000947	Must start a word
68	youngster	0.000987	Must start a word

---

 TABLE 6. Rejections of the manifold hypothesis for Llemma7B

Number	Token	<i>p</i> -value	Comment
1	closure	0.00000000434	
2	agu	0.000000846	
3	¡Cyrillic¿	0.000000938	Must start a word
4	custom	0.00000163	
5	kW	0.00000496	Must start a word
6	}^{{-}}	0.00000833	
7	porque	0.0000128	Must start a word
8	Leopold	0.0000135	Must start a word
9	Rem	0.0000232	Must start a word
10	Ern	0.0000265	Must start a word
11	though	0.0000540	Must start a word
12	č	0.0000619	Must start a word
13	endl	0.0000683	Must start a word
14	corrected	0.0000738	Must start a word
15	tw	0.0000788	Must start a word
16	ères	0.000115	
17	grep	0.000151	
18	kind	0.000202	Must start a word
19	pax	0.000243	
20	Tri	0.000250	Must start a word
21	spielte	0.000258	Must start a word
22	Heaven	0.000262	Must start a word
23	d	0.000289	
24	¡Cyrillic¿	0.000320	
25	Card	0.000335	Must start a word
26	Wall	0.000351	Must start a word
27	periodic	0.000359	Must start a word
28	ucht	0.000463	
29	jeu	0.000553	Must start a word
30	slightly	0.000807	Must start a word
31	passion	0.000823	Must start a word
32	Charles	0.000833	Must start a word
33	victory	0.000906	Must start a word

TABLE 7. Rejections of the manifold hypothesis for Mistral7B

Number	Token	p-value	Comment
1	CV	0.000000241	Must start a word
2	ember	0.00000199	
3	¡Korean character¿	0.00000224	
4	ÿ	0.00000770	
5	rise	0.0000283	Must start a word
6	poured	0.0000305	Must start a word
7	aimed	0.0000364	Must start a word
8	allocate	0.0000553	Must start a word
9	UINT	0.0000684	
10	monitor	0.0000767	Must start a word
11	¡Cyrillic¿	0.000105	
12	\u0006	0.000132	
13	¡Chinese character¿	0.000133	
14	Lat	0.000139	Must start a word
15	Vel	0.000148	
16	challenges	0.000178	Must start a word
17	¡Chinese character¿	0.000200	
18	Od	0.000222	Must start a word
19	neys	0.000244	
20	selon	0.000244	Must start a word
21	measures	0.000268	Must start a word
22	assumes	0.000321	Must start a word
23	Et	0.000338	Must start a word
24	Rot	0.000438	
25	¡Chinese character¿	0.000538	
26	olutely	0.000540	
27	HO	0.000567	
28	Solutions	0.000598	Must start a word
29	*	0.000658	
30	Condition	0.000665	
31	zt	0.000677	
32	iced	0.000696	
33	URL	0.000722	
34	SEO	0.000728	Must start a word
35	weigh	0.000728	Must start a word
36	�nge	0.000765	
37	Vic	0.000777	Must start a word
38	apparent	0.000780	Must start a word
39	¡Chinese character¿	0.000896	
40	¡0xE3¿	0.000921	

---

TABLE 8. Rejections of the manifold hypothesis for Pythia6.9B (1 of 2)

Number	Token	<i>p</i> -value	Comment
1	psychotic	0.000000161	Must start a word
2	\](	0.00000147	
3	1990	0.00000231	
4	tiene	0.00000282	Must start a word
5	ucky	0.0000134	
6	Hebrew	0.0000141	Must start a word
7	mess	0.0000184	
8	reasonable	0.0000300	Must start a word
9	collector	0.0000311	Must start a word
10	embodiments	0.0000428	Must start a word
11	Inhibition	0.0000593	Must start a word
12	Hers	0.0000691	Must start a word
13	odge	0.000120	
14	áQIJ	0.000144	
15	íGíč	0.000165	
16	198	0.000170	Must start a word
17	scare	0.000192	Must start a word
18	]{}\\-[	0.000202	
19	LIMITED	0.000212	Must start a word
20	hop	0.000232	Must start a word
21	BIO	0.000246	
22	raison	0.000252	Must start a word
23	inside	0.000254	
24	st	0.000261	
25	waving	0.000286	Must start a word
26	Austria	0.000287	Must start a word
27	ny	0.000313	

---

TABLE 9. Rejections of the manifold hypothesis for Pythia6.9B (2 of 2)

Number	Token	p-value	Comment
28	bags	0.000326	
29	medium	0.000372	
30	incent	0.000378	Must start a word
31	carboh	0.000407	Must start a word
32	secret	0.000451	Must start a word
33	¡Unicode characters¿	0.000468	
34	ÏGÎp	0.000519	Must start a word
35	120	0.000536	
36	wastes	0.000565	Must start a word
37	ressor	0.000570	
38	Lip	0.000597	Must start a word
39	preview	0.000650	
40	redund	0.000653	Must start a word
41	ridic	0.000673	Must start a word
42	Ramirez	0.000698	Must start a word
43	omatic	0.000707	
44	Gloria	0.000733	Must start a word
45	eton	0.000780	
46	chairman	0.000789	Must start a word
47	Supreme	0.000859	Must start a word
48	grazing	0.000890	Must start a word
49	activation	0.000892	Must start a word
50	imming	0.000914	
51	radiological	0.000931	Must start a word
52	branc	0.000941	Must start a word
53	\$\\—\\	0.000942	Must start a word
54	DEFAULT	0.000992	